

Magnetic properties of a mixed spin-1/2 and spin-3/2 Ising model with an uniaxial and biaxial crystal-field potential¹

Michal Jaščur and Jozef Strečka^{*}

*Department of Theoretical Physics and Astrophysics, Faculty of Science,
P. J. Šafárik University, Park Angelinum 9, 041 54 Košice, Slovak Republic*

Abstract

Magnetic properties of a mixed spin-1/2 and spin-3/2 Ising model on honeycomb lattice are investigated within the framework of an exact star-triangle mapping transformation. The particular attention is focused on the effect of uniaxial and biaxial crystal-field potentials that basically influence a magnetic behavior of the spin-3/2 atoms. Our results for basic thermodynamic quantities as well as dynamical time-dependent autocorrelation function indicate a spin tunneling between $|\pm\frac{3}{2}\rangle$ and $|\mp\frac{1}{2}\rangle$ states in two different magnetically ordered phases OP₁ and OP₂, respectively.

Key words: uniaxial and biaxial crystal-field potential, star-triangle transformation, spin dynamics, exact solution

PACS: 75.10.Hk, 05.50.+q

^{*} Corresponding author.

Email addresses: jascur@upjs.sk (Michal Jaščur), jozkos@pobox.sk (Jozef Strečka).

¹ This work was financially supported by the VEGA grant No. 1/2009/05

1 Introduction

During the last decade, a quantum tunneling of magnetization has become among the most actively studied topics in a condensed matter physics. The immense interest aimed at better understanding of this quantum phenomenon has been mainly stimulated by a recent experimental observation of the quantum spin tunneling in a large number of single-molecule magnets (see Ref. [1] and references therein). By the term single-molecule magnet one denotes an assembly of weakly interacting clusters of magnetic metal atoms that usually possess an extraordinary strong magnetic anisotropy. Hence, the single-molecule magnets often provide very good examples of magnetic systems with a strong uniaxial magnetocrystalline anisotropy, i.e. so-called Ising-like spin systems. Of course, the Ising-type interaction by itself cannot be a source of the quantum spin tunneling experimentally observed in these systems. It turns out, however, that this quantum phenomenon arises in the most cases due to the higher-order crystal-field terms. According to a number of experimental and theoretical studies it is now quite well established that the spin tunneling observed in Fe_4 [2], Fe_8 [3], Fe_{19} [4], or Mn_4 [5] clusters originates to a major extent from a second-order biaxial crystal-field potential.

Extensive studies focused on the magnetic properties of small clusters shed light on the effect of single-ion anisotropy terms D (uniaxial anisotropy) and E (biaxial, also called rhombic anisotropy). In contrast to a quite well understood role of both single-ion anisotropies in the small magnetic clusters (zero-dimensional systems), the situation becomes much more complex and also obscure in one- and two-dimensional spin systems. In fact, ground-state

and the APVT grant No. 20-005204.

properties of a spin- S Ising model with the rhombic crystal-field potential E have been only recently examined by Oitmaa and von Brasch within an effective mapping to the transverse Ising model [6]. On the basis of this effective mapping, a zero-temperature quantum critical point can be exactly located in the one-dimensional model, while for the two-dimensional models, they can be estimated with a high numerical accuracy using the linked-cluster expansion method [6,7]. Nevertheless, the magnetic behavior of these models has not been investigated at non-zero temperatures beyond the standard mean-field and effective-field theories [8], random phase approximation [9], or above mentioned linked cluster expansion [10]. It should be stressed that the biaxial anisotropy essentially influences magnetic properties of a large number of polymeric molecular-based magnetic materials, too. From the most obvious examples one could mention: NiF_2 [11], $\text{NiNO}_3 \cdot 6\text{H}_2\text{O}$ [12], $\text{Ni}(\text{CH}_3\text{COO})_2 \cdot 4\text{H}_2\text{O}$ [13], $\text{Mn}(\text{CH}_3\text{COO})_2 \cdot 3\text{H}_2\text{O}$ [14], CoF_2 [15], $\text{CoCl}_2 \cdot 6\text{H}_2\text{O}$ [16] and a series of compounds $\text{Fe}(\text{dc})_2\text{X}$ [17], where X stands for halides and dc for the dithiocarbamate or diselenocarbamate groups, respectively.

In this article, we will focus on the effect of uniaxial and biaxial crystal-field potentials affecting the magnetic behavior of mixed spin-1/2 and spin-3/2 honeycomb lattice. When assuming the Ising-type exchange interaction between nearest neighbors, the model becomes exactly solvable within an extended star-triangle mapping transformation. Thus, the considered model provides a noble example of statistical system, which enables to study an interplay between quantum effects and temperature in a spontaneously ordered magnetic system. Moreover, a magnetic structure of the mixed-spin honeycomb lattice occurs rather frequently also in the molecular magnetism, what clearly demonstrates a large family of polymeric two-dimensional compounds of fol-

lowing chemical formula: $A^I M^{II} M^{III} (C_2O_4)_3$ [18], where A^I stands for a non-magnetic univalent cation $N(C_n H_{2n+1})_4$ or $P(C_n H_{2n+1})_4$ ($n = 3 - 5$), M^{II} and M^{III} denote two- and three-valent metal atoms $Cu^{II}(S = 1/2)$, $Ni^{II}(S = 1)$, $Co^{II}(S = 3/2)$, $Fe^{II}(S = 2)$ or $Mn^{II}(S = 5/2)$ and respectively, $Cr^{III}(S = 3/2)$ or $Fe^{III}(S = 5/2)$. Actually, it turns out that the crystal structure of these polymeric molecular-based magnetic materials consists of the well-separated two-dimensional layers, in which regularly alternating M^{II} and M^{III} magnetic metal atoms constitute more or less regular honeycomb lattice (Fig. 1). In consequence of a large magnetocrystalline anisotropy of these materials, one should also expect a relatively strong uniaxial (Ising-like) anisotropy, as it has already been suggested in the theoretical studies based on the effective-field theory and Monte-Carlo simulations [19]. Hence, the magnetic compounds from the family of oxalates $A^I M^{II} M^{III} (C_2O_4)_3$ represent good candidates to be described by the proposed model.

The outline of this paper is as follows. In the next section, a detailed description of the model system is presented and then, some basic aspects of the transformation method will be shown. Section 3 deals with a physical interpretation of the most interesting results and finally, some concluding remarks are drawn in Section 4.

2 Model and method

Let us consider a magnetic structure of the mixed-spin honeycomb lattice, as it is schematically depicted in Fig. 1. To ensure exact tractability of the model system, we will further suppose that the sites of sublattice A are occupied by the spin-1/2 atoms (depicted as full circles), in contrast to the sites of

sublattice B that are occupied by the spin-3/2 atoms (open circles). Assuming the Ising-type exchange interaction J between nearest-neighboring spin pairs only, the total Hamiltonian of the system reads:

$$\hat{\mathcal{H}} = J \sum_{\langle k,j \rangle}^{3N} \hat{S}_k^z \hat{\mu}_j^z + D \sum_{k \in B}^N (\hat{S}_k^z)^2 + E \sum_{k \in B}^N [(\hat{S}_k^x)^2 - (\hat{S}_k^y)^2], \quad (1)$$

where N is a total number of sites at each sublattice, $\hat{\mu}_j^z$ and \hat{S}_k^α ($\alpha = x, y, z$) denote standard spatial components of the spin-1/2 and spin-3/2 operators, respectively. The first summation in Eq. (1) is carried out over nearest-neighboring spin pairs, while the other two summations run over the sites of sublattice B . Apparently, the last two terms D and E are the crystal-field potentials that measure a strength of uniaxial and biaxial anisotropies acting on the spin-3/2 atoms. It is also worthy to note that there is one-to-one correspondence between the Hamiltonian (1) and the effective spin Hamiltonian with three different single-ion anisotropy terms D^x , D^y and D^z :

$$\hat{\mathcal{H}} = J \sum_{\langle k,j \rangle}^{3N} \hat{S}_k^z \hat{\mu}_j^z + D^z \sum_{k \in B}^N (\hat{S}_k^z)^2 + D^x \sum_{k \in B}^N (\hat{S}_k^x)^2 + D^y \sum_{k \in B}^N (\hat{S}_k^y)^2. \quad (2)$$

As a matter of fact, one can easily prove the equivalence between (1) and (2) using following mapping relations between the relevant interaction parameters:

$$D = D^z - \frac{1}{2}(D^x + D^y), \quad \text{and} \quad E = \frac{1}{2}(D^x - D^y). \quad (3)$$

It should be also mentioned here that by neglecting the biaxial anisotropy, i.e. setting $E = 0$ in Eq. (1) or equivalently $D^x = D^y$ in Eq. (2), our model reduces to the exactly soluble model settled by Gonçalves [20] several years ago. Accordingly, the main attention will be focused here on the effect of biaxial anisotropy, which influences thermodynamical and dynamical properties

in a crucial manner. Really, the E -term related to the biaxial crystal-field anisotropy should cause non-trivial quantum effects, since it introduces the x and y components of spin operators into the Hamiltonian (1). As a result, it is responsible for the onset of local quantum fluctuations that are obviously missing in the Ising model with the uniaxial crystal-field potential D only.

It is therefore of interest to discuss an origin of the biaxial crystal-field potential E . The origin of this anisotropy term consists in the low-symmetry crystal field of ligands from the local neighborhood of the spin-3/2 atoms. It is noticeable that a threefold symmetry axis oriented perpendicular to the honeycomb layer prevents an appearance of biaxial crystal-field potential in a regular honeycomb lattice with a perfect arrangement of the oxalato groups, as well as magnetic metal atoms. However, a small lattice distortion which occurs rather frequently in the low-dimensional polymeric compounds due to the Jahn-Teller effect can potentially lower the local symmetry. In consequence of that, the distortion of lattice parameters can be regarded as a possible source of the biaxial crystal-field anisotropy. The most obvious example, where the lattice distortion removes the threefold symmetry axis represents the single-molecule magnet Fe_4 , in which three outer Fe atoms occupy two non-equivalent positions around one central Fe atom [2].

Let us turn our attention to the main points of the transformation method, which enables an exact treatment of the model system. Firstly, it is very convenient to write the total Hamiltonian (1) as a sum of site Hamiltonians:

$$\hat{\mathcal{H}} = \sum_{k \in B}^N \hat{\mathcal{H}}^{(k)}, \quad (4)$$

where the each site Hamiltonian $\hat{\mathcal{H}}^{(k)}$ involves all interaction terms associated with one spin-3/2 atom residing on the k th site of sublattice B :

$$\hat{\mathcal{H}}^{(k)} = \hat{S}_k^z E_k + (\hat{S}_k^z)^2 D + [(\hat{S}_k^x)^2 - (\hat{S}_k^y)^2] E, \quad (5)$$

with $E_k = J(\hat{\mu}_{k1}^z + \hat{\mu}_{k2}^z + \hat{\mu}_{k3}^z)$. While the Hamiltonians (5) at different sites commute with respect to each other ($[\hat{\mathcal{H}}^{(i)}, \hat{\mathcal{H}}^{(j)}] = 0$, for each $i \neq j$), the partition function of the system can be partially factorized and consequently, rewritten in the form:

$$\mathcal{Z} = \text{Tr}_{\{\mu\}} \prod_{k=1}^N \text{Tr}_{S_k} \exp[-\beta \hat{\mathcal{H}}^{(k)}]. \quad (6)$$

In above, $\beta = 1/(k_B T)$, k_B is Boltzmann's constant, T the absolute temperature, $\text{Tr}_{\{\mu\}}$ means a trace over spin degrees of freedom of sublattice A and Tr_{S_k} stands for a trace over spin states of the k th spin from sublattice B . A crucial step in our procedure represents the calculation of the expression $\text{Tr}_{S_k} \exp[-\beta \hat{\mathcal{H}}^{(k)}]$. With regard to this, let us write the site Hamiltonian (5) in an usual matrix representation:

$$\hat{\mathcal{H}}^{(k)} = \begin{pmatrix} \frac{9D}{4} + \frac{3E_k}{2} & 0 & \sqrt{3}E & 0 \\ 0 & \frac{D}{4} + \frac{E_k}{2} & 0 & \sqrt{3}E \\ \sqrt{3}E & 0 & \frac{D}{4} - \frac{E_k}{2} & 0 \\ 0 & \sqrt{3}E & 0 & \frac{9D}{4} - \frac{3E_k}{2} \end{pmatrix}, \quad (7)$$

in a standard basis of functions $|\pm 3/2\rangle, |\pm 1/2\rangle$ corresponding, respectively, to the four possible spin states $S_k^z = \pm 3/2, \pm 1/2$ of the k th atom from sublattice B . Although it is easy to find eigenvalues of the site Hamiltonian (7), with

respect to further calculation it is more favorable to obtain directly matrix elements of the expression $\exp[-\beta\hat{\mathcal{H}}^{(k)}]$. When adopting the Cauchy integral formula, one readily attains the matrix elements for an arbitrary exponential function of the site Hamiltonian (7):

$$\begin{aligned}
A_{ij} &= \left(\exp[\alpha\hat{\mathcal{H}}^{(k)}]\right)_{ij}, \\
A_{11} &= \exp\left[\alpha\left(\frac{5}{4}D + \frac{1}{2}E_k\right)\right] \left\{ \cosh(a\xi_k^+) + \frac{D + E_k}{\xi_k^+} \sinh(a\xi_k^+) \right\}, \\
A_{22} &= \exp\left[\alpha\left(\frac{5}{4}D - \frac{1}{2}E_k\right)\right] \left\{ \cosh(a\xi_k^-) - \frac{D - E_k}{\xi_k^-} \sinh(a\xi_k^-) \right\}, \\
A_{33} &= \exp\left[\alpha\left(\frac{5}{4}D + \frac{1}{2}E_k\right)\right] \left\{ \cosh(a\xi_k^+) - \frac{D + E_k}{\xi_k^+} \sinh(a\xi_k^+) \right\}, \\
A_{44} &= \exp\left[\alpha\left(\frac{5}{4}D - \frac{1}{2}E_k\right)\right] \left\{ \cosh(a\xi_k^-) + \frac{D - E_k}{\xi_k^-} \sinh(a\xi_k^-) \right\}, \\
A_{13} = A_{31} &= \exp\left[\alpha\left(\frac{5}{4}D + \frac{1}{2}E_k\right)\right] \frac{\sqrt{3}E}{\xi_k^+} \sinh(a\xi_k^+), \\
A_{24} = A_{42} &= \exp\left[\alpha\left(\frac{5}{4}D - \frac{1}{2}E_k\right)\right] \frac{\sqrt{3}E}{\xi_k^-} \sinh(a\xi_k^-), \tag{8}
\end{aligned}$$

where $\xi_k^\pm = \sqrt{(D \pm E_k)^2 + 3E^2}$ and α marks an arbitrary function. After substituting $\alpha = -\beta$ in the set of Eqs. (8), the relevant trace $\text{Tr}_{S_k} \exp[-\beta\hat{\mathcal{H}}^{(k)}]$ can easily be calculated. Moreover, its explicit form immediately implies a possibility of performing the standard star-triangle mapping transformation:

$$\begin{aligned}
\text{Tr}_{S_k} \exp[-\beta\hat{\mathcal{H}}^{(k)}] &= 2 \exp[-5\beta D/4 - \beta E_k/2] \cosh\left(\beta\sqrt{(D + E_k)^2 + 3E^2}\right) \\
&\quad + 2 \exp[-5\beta D/4 + \beta E_k/2] \cosh\left(\beta\sqrt{(D - E_k)^2 + 3E^2}\right) = \\
&= A \exp\left[\beta R(\mu_{k1}^z \mu_{k2}^z + \mu_{k2}^z \mu_{k3}^z + \mu_{k3}^z \mu_{k1}^z)\right], \tag{9}
\end{aligned}$$

which replaces the partition function of a *star* (i.e. the four-spin cluster consisting of one central spin-3/2 atom and its three nearest-neighboring spin-1/2 atoms) by the partition function of a *triangle* (i.e. the three-spin cluster comprising of three outer spin-1/2 atoms in the corners of equilateral triangle), as shown in Fig. 1. A physical meaning of the mapping (9) is to remove all

interaction parameters associated with the central spin-3/2 atom and to replace them by the effective interaction R between the outer spin-1/2 atoms. It is noteworthy that both mapping parameters A and R are "self-consistently" given by the transformation equation (9), which must be valid for any combination of spin states of three spin-1/2 atoms. In consequence of that, the transformation parameters A and R can be expressed as:

$$A = (\Phi_1 \Phi_2^3)^{1/4}, \quad \beta R = \ln\left(\frac{\Phi_1}{\Phi_2}\right), \quad (10)$$

where the functions Φ_1 and Φ_2 are defined as follows:

$$\begin{aligned} \Phi_1 &= 2 \exp(-5\beta D/4 - 3\beta J/4) \cosh\left(\beta \sqrt{(3J/2 + D)^2 + 3E^2}\right) \\ &\quad + 2 \exp(-5\beta D/4 + 3\beta J/4) \cosh\left(\beta \sqrt{(3J/2 - D)^2 + 3E^2}\right), \\ \Phi_2 &= 2 \exp(-5\beta D/4 - \beta J/4) \cosh\left(\beta \sqrt{(J/2 + D)^2 + 3E^2}\right) \\ &\quad + 2 \exp(-5\beta D/4 + \beta J/4) \cosh\left(\beta \sqrt{(J/2 - D)^2 + 3E^2}\right). \end{aligned} \quad (11)$$

When the mapping (9) is performed at each site of the sublattice B , the original mixed-spin honeycomb lattice is mapped onto the spin-1/2 Ising triangular lattice with the effective interaction R given by the "self-consistency" condition (10)-(11). Indeed, the substitution of equation (9) into the partition function (6) establishes the relationship:

$$\mathcal{Z}(\beta, J, D, E) = A^N \mathcal{Z}_t(\beta, R), \quad (12)$$

between the partition function \mathcal{Z} of the mixed-spin honeycomb lattice and the partition function \mathcal{Z}_t of the corresponding spin-1/2 triangular lattice. Above equation constitutes the basic result of our calculation, since it enables relatively simple derivation of all required quantities, such as the magnetization, quadrupolar moment, correlation function, internal energy, specific heat, etc.

In addition, by combining (12) with (9) one readily proves a validity of following exact spin identities:

$$\langle f_1(\mu_i^z, \mu_j^z, \dots, \mu_k^z) \rangle = \langle f_1(\mu_i^z, \mu_j^z, \dots, \mu_k^z) \rangle_t, \quad (13)$$

$$\begin{aligned} \langle f_2(S_k^x, S_k^y, S_k^z, \mu_{k1}^z, \mu_{k2}^z, \mu_{k3}^z) \rangle &= \\ &= \left\langle \frac{\text{Tr}_{S_k} f_2(S_k^x, S_k^y, S_k^z, \mu_{k1}^z, \mu_{k2}^z, \mu_{k3}^z) \exp[-\beta \hat{\mathcal{H}}^{(k)}]}{\text{Tr}_{S_k} \exp[-\beta \hat{\mathcal{H}}^{(k)}]} \right\rangle, \end{aligned} \quad (14)$$

where $\langle \dots \rangle$ represents the standard canonical average over the ensemble defined by the Hamiltonian (1) and $\langle \dots \rangle_t$ the one performed on the spin-1/2 Ising triangular lattice with the effective exchange interaction R . Here, f_1 is an arbitrary function of the spin variables belonging to the sublattice A , while f_2 denotes an arbitrary function depending on the k th spin of sublattice B and its three nearest neighbors from the sublattice A . By applying the spin identity (13), one straightforwardly attains the following results:

$$m_A \equiv \langle \hat{\mu}_{k1}^z \rangle = \langle \hat{\mu}_{k1}^z \rangle_t \equiv m_t, \quad (15)$$

$$c_A \equiv \langle \hat{\mu}_{k1}^z \hat{\mu}_{k2}^z \rangle = \langle \hat{\mu}_{k1}^z \hat{\mu}_{k2}^z \rangle_t \equiv c_t, \quad (16)$$

$$t_A \equiv \langle \hat{\mu}_{k1}^z \hat{\mu}_{k2}^z \hat{\mu}_{k3}^z \rangle = \langle \hat{\mu}_{k1}^z \hat{\mu}_{k2}^z \hat{\mu}_{k3}^z \rangle_t \equiv t_t, \quad (17)$$

whereas the second spin identity (14) enables after some algebra derivation of quantities depending on the spin variable from the sublattice B :

$$m_B \equiv \langle \hat{S}_k^z \rangle = -3m_A(K_1 + K_2)/2 - 2t_A(K_1 - 3K_2), \quad (18)$$

$$\eta \equiv \langle (\hat{S}_k^z)^2 \rangle = (K_3 + 3K_4)/4 + 3c_A(K_3 - K_4). \quad (19)$$

In above, m_A (m_B) labels the single-site magnetization of the sublattice A (B), η denotes the quadrupolar moment and finally, c_A and t_A stand, respectively, for the static pair and triplet correlation functions between the relevant spins of sublattice A . Obviously, the exact solution of both sublattice magnetization and quadrupolar moment require only a knowledge of the single-site magnetization m_t , nearest-neighbour pair correlation function c_t and triplet

correlation function t_t on the corresponding spin-1/2 Ising triangular lattice unambiguously given by R (10)-(11). Fortunately, the appropriate exact solution of these quantities is well known, hence, one can directly utilize final results derived in Refs. [21]. Finally, the coefficients emerging in the previous set of Eqs. (17)-(20) are listed below:

$$\begin{aligned} K_1 &= F_1(3J/2 + D, 3J/2 - D, 3J/2), & K_2 &= F_1(J/2 + D, J/2 - D, J/2), \\ K_3 &= F_2(3J/2 + D, 3J/2 - D, 3J/2), & K_4 &= F_2(J/2 + D, J/2 - D, J/2), \end{aligned} \quad (20)$$

where the functions $F_1(x, y, z)$ and $F_2(x, y, z)$ are defined as follows:

$$\begin{aligned} F_1(x, y, z) &= \frac{x}{\sqrt{x^2 + 3E^2}} \frac{\sinh(\beta\sqrt{x^2 + 3E^2})}{\cosh(\beta\sqrt{x^2 + 3E^2}) + \exp(\beta z) \cosh(\beta\sqrt{y^2 + 3E^2})} \\ &+ \frac{y}{\sqrt{y^2 + 3E^2}} \frac{\sinh(\beta\sqrt{y^2 + 3E^2})}{\exp(-\beta z) \cosh(\beta\sqrt{x^2 + 3E^2}) + \cosh(\beta\sqrt{y^2 + 3E^2})} \\ &- \frac{1}{2} \frac{\cosh(\beta\sqrt{x^2 + 3E^2}) - \exp(\beta z) \cosh(\beta\sqrt{y^2 + 3E^2})}{\cosh(\beta\sqrt{x^2 + 3E^2}) + \exp(\beta z) \cosh(\beta\sqrt{y^2 + 3E^2})}, \\ F_2(x, y, z) &= \frac{y}{\sqrt{y^2 + 3E^2}} \frac{\sinh(\beta\sqrt{y^2 + 3E^2})}{\exp(-\beta z) \cosh(\beta\sqrt{x^2 + 3E^2}) + \cosh(\beta\sqrt{y^2 + 3E^2})} \\ &+ \frac{5}{4} - \frac{x}{\sqrt{x^2 + 3E^2}} \frac{\sinh(\beta\sqrt{x^2 + 3E^2})}{\cosh(\beta\sqrt{x^2 + 3E^2}) + \exp(\beta z) \cosh(\beta\sqrt{y^2 + 3E^2})}. \end{aligned} \quad (21)$$

Now, we will derive an exact result for one dynamical quantity, namely, the time-dependent autocorrelation function. It should be noted here that exactly tractable models offer only seldom a possibility to investigate their spin dynamics. On the other hand, the dynamical quantities such as autocorrelation and correlation functions are important also from the experimental point of view, because their magnitude directly determines a scattering cross section measured in inelastic neutron scattering experiments [22], or a spin-lattice relaxation rate provided by a nuclear magnetic resonance technique [23].

As a starting point for calculation of the time-dependent autocorrelation function C_{auto}^{zz} can, for convenience, serve the exact spin identity (14):

$$\begin{aligned} C_{auto}^{zz}(t) &\equiv \frac{1}{2} \langle \hat{S}_k^z(0) \hat{S}_k^z(t) + \hat{S}_k^z(t) \hat{S}_k^z(0) \rangle = \\ &= \frac{1}{2} \left\langle \frac{\text{Tr}_{S_k} \{ [\hat{S}_k^z(0) \hat{S}_k^z(t) + \hat{S}_k^z(t) \hat{S}_k^z(0)] \exp[-\beta \hat{\mathcal{H}}^{(k)}] \}}{\text{Tr}_{S_k} \exp[-\beta \hat{\mathcal{H}}^{(k)}]} \right\rangle, \end{aligned} \quad (22)$$

where the symmetrized form in the definition of C_{auto}^{zz} is used to construct a Hermitian operator, $\hat{S}_k^z(t) = \exp(\frac{it\hat{\mathcal{H}}_k}{\hbar}) \hat{S}_k^z \exp(-\frac{it\hat{\mathcal{H}}_k}{\hbar})$ represents the Heisenberg picture for the time-dependent operator $\hat{S}_k^z(t)$, \hbar stands for the reduced Planck's constant and $i = \sqrt{-1}$. Next, the matrix elements of expressions $\exp(\pm \frac{it\hat{\mathcal{H}}_k}{\hbar})$ can be in turn evaluated by putting $\alpha = \pm \frac{it}{\hbar}$ into the set of Eqs. (8). Then, after a straightforward but a little bit tedious calculation, one arrives to a final result for the dynamical autocorrelation function:

$$\begin{aligned} C_{auto}^{zz} &= \frac{1}{4} [K_5(D + 3J/2, D - 3J/2, 3J/2) + 3K_6(D + J/2, D - J/2, J/2)] \\ &+ 3c_t [K_5(D + 3J/2, D - 3J/2, 3J/2) - K_6(D + J/2, D - J/2, J/2)], \end{aligned} \quad (23)$$

where the time-dependent coefficients K_5 and K_6 are, for brevity, explicitly given in the Appendix.

3 Results and discussion

Before proceeding to a discussion of the most interesting results, it is noticeable that the results derived in the previous section are rather general, since they are valid for a ferromagnetic ($J < 0$) as well as ferrimagnetic ($J > 0$) version of the model under investigation. In what follows, we shall restrict our analysis to the ferrimagnetic model only, since the polymeric compounds from the family of oxalates [18] fall mostly into the class of ferrimagnets. Nev-

ertheless, it appears worthwhile to remark that a magnetic behavior of the ferrimagnetic system completely resembles the one of ferromagnetic system. Finally, one should also emphasize that the mapping (9) remains invariant under the transformation $E \leftrightarrow -E$. For this reason, one may consider without loss of generality the parameter $E \geq 0$ and consequently, x -, y - and z -axis then represent the hard-, medium- and easy-axis for a given system.

3.1 Ground-state properties

At first, we will take a closer look at the ground-state behaviour. Taking into account the zero-temperature limit ($T \rightarrow 0^+$), one finds the following condition for a first-order phase transition line separating two different magnetically ordered phases denoted as OP_1 and OP_2 :

$$\frac{D}{J} = \sqrt{\left(\frac{3}{4}\right)^2 + \left(\frac{E}{J}\right)^2}. \quad (24)$$

Moreover, one easily attains from Eqs. (15)-(21) analytical results for the single-site sublattice magnetization (m_A, m_B) , the total magnetization normalized per one magnetic atom $m = (m_A + m_B)/2$ and the quadrupolar moment η , as well:

$$\begin{aligned} OP_1: \quad m_A &= -\frac{1}{2}, \quad m_B = \frac{1}{2} + \frac{\frac{3}{2} - \frac{D}{J}}{\sqrt{\left(\frac{3}{2} - \frac{D}{J}\right)^2 + 3\left(\frac{E}{J}\right)^2}}, \\ m &= \frac{1}{2} \frac{\frac{3}{2} - \frac{D}{J}}{\sqrt{\left(\frac{3}{2} - \frac{D}{J}\right)^2 + 3\left(\frac{E}{J}\right)^2}}, \quad \eta = \frac{5}{4} + \frac{\frac{3}{2} - \frac{D}{J}}{\sqrt{\left(\frac{3}{2} - \frac{D}{J}\right)^2 + 3\left(\frac{E}{J}\right)^2}}; \end{aligned} \quad (25)$$

$$OP_2: \quad m_A = -\frac{1}{2}, \quad m_B = -\frac{1}{2} + \frac{\frac{3}{2} + \frac{D}{J}}{\sqrt{\left(\frac{3}{2} + \frac{D}{J}\right)^2 + 3\left(\frac{E}{J}\right)^2}}, \quad (26)$$

$$m = -\frac{1}{2} - \frac{1}{2} \frac{\frac{3}{2} - \frac{D}{J}}{\sqrt{\left(\frac{3}{2} - \frac{D}{J}\right)^2 + 3\left(\frac{E}{J}\right)^2}}, \quad \eta = \frac{5}{4} - \frac{\frac{3}{2} + \frac{D}{J}}{\sqrt{\left(\frac{3}{2} + \frac{D}{J}\right)^2 + 3\left(\frac{E}{J}\right)^2}}.$$

For better illustration, Fig. 2 depicts the ground-state phase diagram in the E - D plane (Fig. 2a) and the zero-temperature variations of the magnetization and quadrupolar moment with the biaxial anisotropy when $D/J = 1.0$ (Fig. 2b). It should be mentioned that by neglecting the biaxial anisotropy, i.e. by putting $E/J = 0.0$ into the phase boundary condition (24), one recovers the boundary uniaxial anisotropy $D/J = 0.75$ in accordance with the results reported by Gonçalves [20] several years ago. Moreover, the OP_1 (OP_2) phase corresponds in this limit to the simple ferrimagnetic (antiferromagnetic) phase with both sublattice magnetization oriented antiparallel with respect to each other: $m_A = -0.5$, $m_B = 1.5$ in the OP_1 and respectively, $m_A = -0.5$, $m_B = 0.5$ in the OP_2 . Apparently, the spin-3/2 atoms occupy exclusively the $|+3/2\rangle$ ($|+1/2\rangle$) state in the OP_1 (OP_2) phase when $E = 0$ is satisfied.

The situation becomes much more complex by turning on the biaxial anisotropy. Even though the sublattice magnetization m_A remains in the ground-state at its saturation value in both OP_1 and OP_2 phases, the sublattice magnetization m_B is gradually suppressed by the effect of biaxial anisotropy (see Fig. 2b). It is quite obvious from this figure that the biaxial anisotropy gradually destroys the perfect ferrimagnetic (antiferromagnetic) spin arrangement, which occurs in the OP_1 (OP_2) phase in the limit of vanishing E . Let us find a primary occasion for this unexpected behavior accompanied by a spin reduction at sublattice B . According to Eq. (26), one finds $\eta - m_B = 3/4$ to be valid in the whole parameter space corresponding to the OP_1 . From an elementary consideration it can be easily understood that the spin-3/2 atoms must occupy in the OP_1 phase either the $|+3/2\rangle$ or $| - 1/2\rangle$ state in order to satisfy

simultaneously both values of m_B and η in the ground state. Aforementioned argument is also supported by the fact that the E -term does not couple in the Hamiltonian (7) the $|+3/2\rangle$ and $| - 1/2\rangle$ states with the $|+1/2\rangle$ and $| - 3/2\rangle$ ones. Hence, the $|+3/2\rangle$ and $| - 1/2\rangle$ states are in the OP_1 phase the only *allowable* states, while the $|+1/2\rangle$ and $| - 3/2\rangle$ states are, on the contrary, the *forbidden* ones. The observed spin reduction at sublattice B can be thus attributed to the local quantum fluctuations induced by the biaxial anisotropy, which in turn lead to a spin tunneling between the $|+3/2\rangle$ and $| - 1/2\rangle$ states in the OP_1 . Although the occupation of the minority $| - 1/2\rangle$ state rises steadily with increasing the biaxial anisotropy strength, it is noticeable that the $|+3/2\rangle$ state still remains the state with the most probable occupation. For completeness, it should be pointed out that in accord with our expectation the negative uniaxial anisotropy ($D < 0$) reduces the occupation of the minority $| - 1/2\rangle$ state, while the positive one ($D > 0$) favors it.

Quite similar situation emerges also in the OP_2 phase. However, it is worthwhile to remark that the OP_2 phase appears in the region of strong uniaxial anisotropies $D/J > 0.75$ only. Due to a strong positive uniaxial anisotropy, the spin-3/2 atoms undergo a well-known spin transition from the $|+3/2\rangle$ to $|+1/2\rangle$ state, which macroscopically manifests itself in the phase transition from the OP_1 to OP_2 phase. As stated before, the biaxial anisotropy couples together the $|+1/2\rangle$ and $| - 3/2\rangle$ states and therefore, the tunneling between these spin states should be expected to occur in the OP_2 . The analytical solution for m_B and η (27), as well as a validity of the relation $\eta + m_B = 3/4$ in a whole parameter space corresponding to the OP_2 phase, indeed confirm this suggestion. However, the negative (positive) uniaxial anisotropy prefers (reduces) the occupation of minority $| - 3/2\rangle$ state in the OP_2 phase in contrast

to the abovementioned trends observed in the OP_1 phase.

Now, let us step forward to the discussion of the time dependent autocorrelation function (23). Among other matters, this quantity can serve in evidence whether the spin-3/2 atoms fluctuate in the OP_1 (OP_2) phase between their *allowable* $|+3/2\rangle$ and $|-1/2\rangle$ ($|+1/2\rangle$ and $|-3/2\rangle$) spin states. Unfortunately, it is quite tedious to derive from Eq. (23) a simple analytical expression for C_{auto}^{zz} in the zero-temperature limit, hence, we report for C_{auto}^{zz} numerical results obtained at very low temperature ($k_B T/J = 0.001$) close to the ground state. Fig. 3 displays the time variation of C_{auto}^{zz} for several values of uniaxial and biaxial crystal-field potentials. Since C_{auto}^{zz} evidently varies in time, it clearly demonstrates the zero-temperature spin dynamics between the *allowable* states. Moreover, a detailed analysis reveals that C_{auto}^{zz} is in the zero-temperature limit a harmonic function of time and whence, the time dependence can be characterized by an angular frequency $\omega_{\pm} = \frac{2J}{\hbar} \sqrt{(\frac{D}{J} \pm 1) + 3(\frac{E}{J})^2}$ depending on whether the system resides the OP_1 , or OP_2 phase. This result is taken to mean that the spin system necessarily recovers after some characteristic recurrence time ($\tau_{\pm} = 2\pi/\omega_{\pm}$) its initial state. More specifically, Fig. 3a illustrates the time variation of C_{auto}^{zz} in the OP_1 phase, because with respect to Eq. (24) one never approaches the OP_2 phase for $D/J = 0.0$. Fig. 3a clearly clarifies the role of biaxial anisotropy: the stronger the biaxial anisotropy E/J , the greater the angular frequency of spin tunneling and in the consequence of that, the shorter the appropriate recurrence time. Furthermore, the increasing strength of the biaxial anisotropy enhances also the amplitude of oscillation in the time-dependence of C_{auto}^{zz} . This observation would suggest that the increase of biaxial anisotropy enhances a number of the spin-3/2 atoms tunneling during the recurrence time between the $|+3/2\rangle$ and $|-1/2\rangle$ states in the OP_1

phase. However, since the equilibrium magnetization does not change in time, the number of atoms that tunnel from $|+3/2\rangle$ to $|-1/2\rangle$ state must definitely be the same as those that tunnel from the $|-1/2\rangle$ to $|+3/2\rangle$ state.

To illustrate the effect of uniaxial anisotropy, the time variation of C_{auto}^{zz} is shown in Fig. 3b for $E/J = 0.5$ and several values of D/J . Apparently, the C_{auto}^{zz} oscillates for strong negative (positive) uniaxial constants D/J in the vicinity of boundary values $C_{auto}^{zz} = 2.25(0.25)$. These values clearly demonstrate that the prevailing number of spin-3/2 atoms occupy in the OP₁ (OP₂) phase the $|+3/2\rangle$ ($|+1/2\rangle$) state, since $C_{auto}^{zz} = \eta$ when $t = 0$. Moreover, the stronger the uniaxial anisotropy (independently of its sign), the smaller the relevant amplitudes of oscillation, i.e. the smaller the number of tunneling atoms during the recurrence time. On the other hand, the increasing strength of uniaxial anisotropy enhances the angular frequency of oscillation, what means, that the tunneling atoms return from the minority $|-1/2\rangle$ ($|-3/2\rangle$) state to the most probable occupied $|+3/2\rangle$ ($|+1/2\rangle$) state of the OP₁ (OP₂) phase after a shorter recurrence time.

3.2 *Finite-temperature behaviour*

In this part, we would like to comment on the finite-temperature behaviour of the system under investigation. Let us begin by considering the effect of uniaxial and biaxial single-ion anisotropies on the critical behaviour. For this purpose, two typical finite-temperature phase diagrams are illustrated in Fig. 4a and 4b. In both figures, the OP₁ (OP₂) phase can be located below the phase boundaries depicted as solid (dashed) lines, while above these boundary lines the usual paramagnetic phase becomes stable. Further, open circles represent

special critical points at which both OP_1 and OP_2 phases coexist. Actually, we have not found any phase transition between the OP_1 and OP_2 phases at non-zero temperatures, what indicates that the OP_1 phase coexists with the OP_2 one at non-zero temperatures merely for the same $D/J - E/J$ values as in the ground state (24). Finally, a closer mathematical analysis reveals that both temperature-driven phase transitions which are related to the OP_1 and OP_2 phase, respectively, are of a second order and belong to a standard Ising universality class.

Fig. 4a shows the critical temperature (T_c) as a function of the uniaxial anisotropy for several values of the biaxial anisotropy. The critical temperature versus uniaxial anisotropy dependence is quite obvious for $E/J = 0.0$, when increasing D/J , T_c monotonically decreases. Hence, the critical temperature approaches in the limit $D/J \rightarrow -\infty(+\infty)$ its minimum (maximum) value $k_B T_c/J = 0.3796\dots$ ($1.1389\dots$) in agreement with the exact T_c (triple T_c) of the spin-1/2 Ising honeycomb lattice. A gradual decline of the transition temperature can obviously be explained as a consequence of the fact, that the positive uniaxial anisotropy energetically favors the low-spin $|\pm 1/2\rangle$ states before the high-spin $|\pm 3/2\rangle$ ones. The most interesting finding to emerge here is that the biaxial anisotropy may significantly modify the critical behavior of the studied system. As a matter of fact, T_c firstly reaches its local minimum at certain positive D/J and then rises steadily to its limiting value $k_B T_c/J = 0.3796\dots$. The extraordinary increase of T_c in the region $D/J > 1.0$ can be explained through a suppression of the occupation of minority $|-3/2\rangle$ state, which appears in the OP_2 phase due to the uniaxial anisotropy effect. In accordance with previous assumption, the greater the biaxial anisotropy (i.e. the greater a number of atoms that occupy the minority $|-3/2\rangle$ state), the

more impressive increase of T_c can be observed. In addition, it is easy to understand from here that the biaxial anisotropy substantially lowers the critical temperature of OP_1 phase in the $D/J \leq 0.0$ region, in that it is responsible for the quantum spin tunneling between the $|+3/2\rangle$ and $|-1/2\rangle$ states.

To illustrate the influence of biaxial anisotropy on the criticality, the dependence of transition temperature on the biaxial anisotropy is shown in Fig. 4b for several values of the uniaxial anisotropy D/J . As one would expect, T_c gradually decreases with increasing the biaxial anisotropy for any $D/J < 0.75$. It is quite obvious that the appropriate suppression of T_c can be attributed to the quantum fluctuations, which become the stronger, the greater the ratio E/J . Apart from this rather trivial finding, one also observes here the peculiar dependences with the non-monotonic behavior of T_c . The critical temperature may exhibit only a slight variation with increasing E/J (as it is in the case of $D/J = 1.0$), or it may show unexpected local minima, as it is in the case of $D/J = 2.0$ and 3.0 . Since the local minima can be located very near to the coexistence point of the OP_1 and OP_2 phases (depicted as open circles), the relevant increase of T_c can be related to the $OP_2 \rightarrow OP_1$ phase transition. Namely, the most populated $|+1/2\rangle$ spin state in the OP_2 is replaced after this phase transition by the $|+3/2\rangle$ state, which is the most occupied spin state in the OP_1 . The spin crossover from the low-spin $|+1/2\rangle$ to the high-spin $|+3/2\rangle$ state must lead, of course, to a slight increase of T_c .

At this stage, let us provide an independent check of the critical behavior by studying thermal dependences of magnetization. The single-site magnetization is plotted against temperature in Fig. 5 for the biaxial anisotropy $E/J = 0.5$ and several values of the uniaxial anisotropy D/J . Fig. 5a shows a typical situation observed in the OP_1 phase: the more positive the uniaxial crystal-field

potential D/J , the stronger the spin reduction (the lower the magnetization m_B) due to the $|+3/2\rangle \leftrightarrow |-1/2\rangle$ spin tunneling. In consequence of that, the total magnetization alters from a standard Q-type dependence observed for $D \leq 0$ (see for instance the curves for $D/J = -2.0$ and 0.0) to a more interesting R-type dependence, which occurs for positive uniaxial anisotropies ($D/J = 0.5$ and 0.75). Unusual slope in the thermal dependence of total magnetization can be related to a more rapid thermal variation of m_B . In fact, on account of the quantum fluctuations m_B is thermally easier disturbed than m_A which, on the contrary, always exhibits the standard Q-type behavior (spin-1/2 atoms are not directly affected by the biaxial crystal-field potential E). Furthermore, Fig. 5b shows how the situation changes by considering the transition toward the OP₂ phase. Actually, both magnetically ordered phases OP₁ and OP₂ have the same internal energy (coexist together) at $D/J = \sqrt{13}/4$ when $E/J = 0.5$, while the OP₂ phase becomes more stable if $D/J > \sqrt{13}/4$. Accordingly, Fig. 4b displays the thermal variation of sublattice magnetization exactly at the OP₁-OP₂ phase boundary and in the OP₂ phase ($D/J = 1.0$ and 1.5). The corresponding thermal dependences of total magnetization are plotted in the insert of Fig. 5b. As it is apparent from these figures, the initial value of m_B is suppressed from its saturation value ($m_B = 0.5$) owing to a presence of the minority $|-3/2\rangle$ state. Nevertheless, a large number of spins can be thermally excited to the $|+3/2\rangle$ state for D/J from the vicinity of OP₁-OP₂ phase boundary and hence, m_B rapidly increases upon heating (see the curve for $D/J = 1.0$). As a result of this thermal excitation, the total magnetization exhibits N-type dependence with one compensation point in which m_A and m_B completely cancel out (see the insert in Fig. 5b). Finally, even for stronger uniaxial anisotropies (e.g. $D/J = 1.5$) the total magnetization recovers the Q-shape, since the thermal fluctuation prefer excitations to

the $| - 1/2 \rangle$ state rather than to the $| + 3/2 \rangle$ one. Such a thermal excitations must, naturally, lower the sublattice magnetization m_B .

To conclude our discussion devoted to finite-temperature properties, let us proceed to the time variation of dynamical autocorrelation function C_{auto}^{zz} as depicted in Fig. 6 for $E/J = 0.5$ and three selected values of D/J . In order to enable a comparison between the displayed data at various D/J , the relevant temperatures are normalized with respect to their appropriate critical temperatures, i.e. we have defined the dimensionless temperature $\tau = T/T_c$ that measures a difference from the critical point ($\tau_c = 1.0$). The time variations of C_{auto}^{zz} from Fig. 6a and 6b display the relevant changes of dynamical autocorrelation function in the OP₁ phase, while Fig. 6c shows the corresponding dependences in the OP₂ phase. It can be easily understood that C_{auto}^{zz} is not in general the time-periodic function at non-zero temperatures no matter whether considering C_{auto}^{zz} in the OP₁, or OP₂ phase. In fact, C_{auto}^{zz} arises according to Eq. (23) as a superposition of two harmonic oscillations with two different angular frequencies $\omega_{\pm} = \frac{2J}{\hbar} \sqrt{(\frac{D}{J} \pm 1)^2 + 3(\frac{E}{J})^2}$ and also various amplitudes. The interference between these harmonic oscillations gives rise to a rather complex time variation of C_{auto}^{zz} , which is in general aperiodic, displaying nodes and other typical interference effects. The periodicity of C_{auto}^{zz} at non-zero temperatures is maintained only for some particular $E/J - D/J$ values, which retain the ratio ω_+/ω_- to be rational, while in any other case, C_{auto}^{zz} behaves aperiodically.

The dependences drawn in Fig. 6 nicely illustrate also the temperature effect on the spin dynamics. It follows from these dependences that some amplitudes are suppressed as the temperature increases, while another ones become more robust. Obviously, in the high-temperature regime that amplitudes be-

come dominant, which coincide to the oscillation with lower angular frequency. Contrary to this, the amplitudes arising from higher frequency oscillation dominate in the low-temperature regime. The most miscellaneous time variation of C_{auto}^{zz} thus emerges in the vicinity of critical temperature ($\tau \approx 1.0$), which represents an intermediate temperature range between the low- and high-temperature regime. However, a rather exceptional case is displayed in Fig. 6c, where the most miscellaneous dependence appears surprisingly at substantially lower temperature ($\tau = 0.25$) rather than the critical one ($\tau_c = 1.0$). When looking back to the thermal variation of magnetization depicted in Fig. 5b, one finds a feasible explanation for this striking behavior. It turns out that the temperature ($\tau \approx 0.25$) of the most miscellaneous time variation of C_{auto}^{zz} coincides with the temperature $k_B T/J \approx 0.1$, at which the most robust spin excitation to the $|+3/2\rangle$ can be observed. In addition to the *allowable* $|+1/2\rangle$ and $| -3/2\rangle$ states, a large number of the spin-3/2 atoms is therefore thermally excited to the $|+3/2\rangle$ spin state. This observation would suggest that the thermal excitations can basically modify the spin dynamics as well.

4 Concluding remarks

In this article, the exact solution of the mixed spin-1/2 and spin-3/2 Ising model on honeycomb lattice is presented and discussed in detail. The particular attention has been focused on the effect of uniaxial and biaxial crystal-field anisotropies acting on the spin-3/2 atoms. As it has been shown, a presence of the biaxial anisotropy significantly modifies the magnetic behavior of the system under investigation. It turns out that already a small amount of the biaxial anisotropy raises a non-trivial spin dynamics and basically influences

the thermodynamic properties, as well.

The most striking finding to emerge here constitutes an exact evidence of the spin tunneling between the $|\pm 3/2\rangle$ and $|\mp 1/2\rangle$ states in two different magnetically ordered phases OP_1 and OP_2 , respectively. Macroscopically, the tunneling effect decreases the critical temperature of the magnetically ordered phases and appreciably suppresses the magnetization of spin-3/2 sublattice. This quantum reduction appears apparently due to the local quantum fluctuations arising from the biaxial crystal-field potential.

There is an interesting correspondence between the model described by the Hamiltonian (1) and a similar model with a local transverse magnetic field Ω acting on the spin-3/2 atoms only [24]. However, similarity in their actual properties is not accidental, in fact, when neglecting the uniaxial crystal-field potential D in Hamiltonian (1), an effective mapping $E \leftrightarrow \Omega$ ensures the equivalence between both the models. Since this mapping is not related to the magnetic structure in any fashion, the appropriate correspondence can be extended to the several lattice models. It is therefore valuable to mention that magnetic properties of the models with a local transverse field become a subject matter of many theoretical works [25]. Apparently, the magnetic behavior of these systems should completely resemble that one of their counterparts with the biaxial crystal-field potential.

Finally, let us turn back to the origin of biaxial anisotropy. Uprise of this anisotropy term in the mixed-spin honeycomb lattice is, namely, closely associated with at least a small lattice distortion. To simplify the situation, the proposed Hamiltonian (1) accounts for the biaxial crystal-field anisotropy, while a difference between exchange interactions in the different spatial direc-

tions has been for simplicity omitted. Nevertheless, the developed procedure can be rather straightforwardly generalized to an anisotropic model accounting for the different interactions along various spatial directions. Moreover, the biaxial anisotropy can be even considered as an arbitrary function (linear, quadratic, exponential, logarithmic, ...) of the ratio between appropriate interaction parameters. Hence, it would be very interesting to find out whether such a system is instable toward the spontaneous lattice distortion caused by the spin-Peierls phenomenon. In this direction continues our next work.

5 Appendix

An explicit form of the coefficients K_5 and K_6 is given by:

$$K_5(x, y, z) = G(x, y, z)/\Phi_1, \quad \text{and} \quad K_6(x, y, z) = G(x, y, z)/\Phi_2,$$

where the function $G(x, y, z)$ is defined as follows:

$$\begin{aligned} G(x, y, z) &= \frac{9}{4}[W_1(x)H_1(x, z) + W_1(y)H_1(y, -z)] + \frac{1}{4}[W_2(x)H_2(x, z) \\ &\quad + W_2(y)H_2(y, -z)] - [W_3(x)H_3(x, z) + W_3(y)H_3(y, -z)], \\ W_1(x) &= \left\{ x^2 + E^2 \left[1 + 2 \cos(2t\sqrt{x^2 + 3E^2}/\hbar) \right] \right\} / (x^2 + 3E^2), \\ W_2(x) &= \left\{ x^2 - 3E^2 \left[1 - 2 \cos(2t\sqrt{x^2 + 3E^2}/\hbar) \right] \right\} / (x^2 + 3E^2), \\ W_3(x) &= \left\{ \sqrt{3}Ex \left[1 - \cos(2t\sqrt{x^2 + 3E^2}/\hbar) \right] \right\} / (x^2 + 3E^2), \\ H_1(x, y) &= \exp(-5\beta D/4 - \beta y/2) \left[\cosh(\beta\sqrt{x^2 + 3E^2}) \right. \\ &\quad \left. - x \sinh(\beta\sqrt{x^2 + 3E^2})/\sqrt{x^2 + 3E^2} \right], \\ H_2(x, y) &= \exp(-5\beta D/4 - \beta y/2) \left[\cosh(\beta\sqrt{x^2 + 3E^2}) \right. \\ &\quad \left. + x \sinh(\beta\sqrt{x^2 + 3E^2})/\sqrt{x^2 + 3E^2} \right], \\ H_3(x, y) &= \exp(-5\beta D/4 - \beta y/2) \sqrt{3}E \sinh(\beta\sqrt{x^2 + 3E^2})/\sqrt{x^2 + 3E^2}. \end{aligned}$$

References

- [1] R. Sessoli and D. Gatteschi, *Angew. Chem.* 42 (2003) 268.
- [2] A. L. Barra, A. Caneschi, A. Cornia, F. Fabrizi de Biani, D. Gatteschi, C. Sangregorio, R. Sessoli and L. Sorace, *J. Am. Chem. Soc.* 121 (1999) 5302;
G. Amoretti, S. Carretta, R. Caciuffo, H. Casalta, A. Cornia, M. Affronte, D. Gatteschi, *Phys. Rev. B* 64 (2001) 104403.
- [3] K. Wieghardt, K. Pohl, I. Jibril, G. Huttner, *Angew. Chem.* 96 (1984) 63;
M. Hennion, L. Pardi, I. Mirebeau, E. Suard, R. Sessoli, A. Caneschi,
Phys. Rev. B 56 (1997) 8819;
R. Sessoli, D. Gatteschi, A. Caneschi, M. A. Novak, *Nature* 365 (1993) 141;
R. Sessoli, *Mol. Cryst. Liq. Cryst.* 274 (1995) 145.
- [4] J. C. Goodwin, R. Sessoli, D. Gatteschi, W. Wernsdorfer, A. K. Powell and
S. L. Health, *J. Chem. Soc. Dalton Trans.* (2000) 1835;
M. Affronte, J. C. Lasjaunias, W. Wernsdorfer, R. Sessoli, D. Gatteschi,
S. L. Health, A. Fort and A. Rettori, *Phys. Rev. B* 66 (2002) 064408.
- [5] W. Wernsdorfer, S. Bhaduri, C. Boskovic, G. Christou and D. N. Hendrickson,
Phys. Rev. B 65 (2002) 180403.
- [6] J. Oitmaa and A. M. A. von Brasch, *Phys. Rev. B* 67 (2003) 172402.
- [7] K. K. Pan and Y.-L. Wang, *Phys. Rev. B* 51 (1995) 3610.
- [8] N. Ch. Eddeqaqi, M. Saber, A. El-Atri and M. Kerouad,
Physica A 272 (1999) 144;
W. Jiang, G. Z. Wei and A. Du, *J. Magn. Magn. Mater.* 250 (2002) 49;
W. Jiang, G. Z. Wei, A. Du and L. Q. Guo, *Physica A* 313 (2002) 503;
W. Jiang, G. Z. Wei and Q. Zhang, *Physica A* 329 (2003) 161.

- [9] G. P. Taggart, R. A. Tahir-Kheli and E. Shiles, *Physica* 75 (1974) 234;
R. Mienas, *Physica A* 89 (1977) 431.
- [10] K. K. Pan and Y.-L. Wang, *Phys. Lett. A* 178 (1993) 325.
- [11] T. Moriya, *Phys. Rev.* 117 (1960) 635.
- [12] L. Berger and S. A. Friedberg, *Phys. Rev.* 136 (1964) A158.
- [13] L. G. Polgar and S. A. Friedberg, *Phys. Rev. B* 6 (1972) 3497.
- [14] H. Kumagai, K. Ôno, I. Hayashi and K. Kambe, *Phys. Rev.* 2 (1952) 374.
- [15] M. E. Lines, *Phys. Rev.* 137 (1965) A982.
- [16] N. Uryû, J. Skalyo and S. A. Friedberg, *Phys. Rev.* 144 (1966) 684.
- [17] G. C. DeFotis, F. Palacio and R. L. Carlin, *Phys. Rev. B* 20 (1979) 2945;
G. C. De Fotis, B. K. Failon, F. V. Wells and H. H. Wickman,
Phys. Rev. B 29 (1984) 3795.
- [18] Z. J. Zhong, N. Matsumoto, H. Ôkawa, S. Kida, *Chem. Lett.* (1990) 87;
H. Tamaki, M. Mitsumi, K. Nakamura, N. Matsumoto, S. Kida, H. Ôkawa and
S. Iijima, *Chem. Lett.* (1992) 1975;
H. Tamaki, Z. J. Zhong, N. Matsumoto, S. Kida, M. Koikawa, Y. Aihwa,
Y. Hashimoto and H. Ôkawa, *J. Am. Chem. Soc.* 114 (1992) 6974;
S. Iijima, T. Katsura, H. Tamaki, M. Mitsumi, N. Matsumoto and H. Ôkawa,
Mol. Cryst. Liq. Cryst. Sci. Technol. A 233 (1993) 263;
S. Decurtins, S. W. Schmalle, H. R. Ostwald, A. Linden, J. Ensling, P. Gütlich
and A. Hauser, *Inorg. Chim. Acta* 216 (1994) 65;
C. Mathonière, S. G. Carling, Y. Dou and P. Day,
J. Chem. Soc. Chem. Commun. (1994) 1554;
W. M. Reiff, J. Kreis, L. Meda and R. U. Kirss,
Mol. Cryst. Liq. Cryst. Sci. Technol. A 273 (1995) 181;

- C. Mathonière, C. J. Nuttall, S. G. Carling and P. Day,
Inorg. Chem. 35 (1996) 1201.
- [19] T. Kaneyoshi, Y. Nakamura and S. Shin,
J. Phys.: Condens. Matter 10 (1998) 7025;
Y. Nakamura, J. Phys.: Condens. Matter 12 (2000) 4067;
Y. Nakamura, Phys. Rev. B 62 (2000) 11742;
Y. Nakamura, Prog. Theor. Phys. 138 (2000) 466;
G. M. Buendia and E. Machado, J. Magn. Magn. Mater. 272-276 (2004) 249.
- [20] L. L. Gonçalves, Physica Scripta 32 (1985) 248;
L. L. Gonçalves, Physica Scripta 33 (1986) 192;
J. W. Tucker, J. Magn. Magn. Mater. 95 (1999) 133.
- [21] R. B. Potts, Phys. Rev. 88 (1952) 352;
G. F. Newell, Phys. Rev. 79 (1950) 876;
R. M. F. Houtappel, Physica 16 (1950) 425;
H. N. V. Temperley, Proc. Roy. Soc. 203A (1950) 202;
R. J. Baxter and T. Choy, Proc. Roy. Soc. London Ser. A 423 (1989) 279;
J. H. Barry, T. Tanaka, M. Khatun and C. H. Múnera,
Phys. Rev. B 44 (1991) 2595.
- [22] E. Balcar, S. W. Lovesey, *Theory of magnetic neutron and photon scattering*,
(Clarendon, Oxford, 1989).
- [23] T. Moriya, Prog. Theor. Phys. 16 (1956) 23.
- [24] M. Jaščur, S. Lacková, J. Phys.: Condens. Matter 12 (2000) L583.
- [25] M. Jaščur, J. Strečka, Phys. Lett. A 258 (1999) 47;
J. Strečka, M. Jaščur, Acta Electrotechnica et Informatica 2 (2002) 102
(cond-mat/0207519);
J. Strečka, H. Čenčariková, M. Jaščur,

Acta Electrotechnica et Informatica 2 (2002) 107 (cond-mat/0207518);

H. Suzuki, M. Suzuki, Int. J. Mod. Phys. B 16 (2002) 3871;

J. Strečka, M. Jaščur, J. Magn. Magn. Mater. 260 (2003) 415;

Y. Fukumoto and A. Oguchi, J. Magn. Magn. Mater. 272-276 (2004) 910.

Figure captions

Fig. 1 The segment of a mixed-spin honeycomb lattice. The lattice positions of the spin-1/2 (spin-3/2) atoms are schematically designated by the full (open) circles, the solid lines label interactions between nearest neighbors. The dashed lines represent the effective interactions between three outer spin-1/2 atoms arising after performing the mapping (9) at k th site.

Fig. 2 a) The ground-state phase diagram in the $E/J - D/J$ plane; b) The single-site sublattice magnetization $|m_A|$ (dotted line) and m_B (dashed line), the total single-site magnetization $|m|$ (solid line) and the quadrupolar momentum η (solid line) as a function of the biaxial anisotropy E/J at $T = 0$ and $D/J = 1.0$.

Fig. 3 The time variation of dynamical autocorrelation function C_{auto}^{zz} at very low temperature ($k_B T/J = 0.001$) close to the ground state: a) for $D/J = 0.0$ and various E/J ; b) for $E/J = 0.5$ and various D/J ; Time axis is scaled in \hbar/J units.

Fig. 4 a) The dependence of critical temperature on the uniaxial anisotropy D/J for several values of biaxial anisotropies E/J ; b) The dependence of critical temperature on the biaxial anisotropy E/J for several values of uniaxial anisotropies D/J . Solid (broken) lines correspond to critical temperatures of the OP₁ (OP₂) phase. Open circles denote the critical temperatures for a such particular case, when both the ordered phases OP₁ and OP₂ coexist in the ground state (see the text).

Fig. 5 The thermal dependences of single-site magnetization for $E/J = 0.5$ and: a) $D/J = -2.0, 0.0, 0.5$ and 0.75 ; b) $D/J = \sqrt{13}/4, 1.0$ and 1.5 . The dotted (dashed)

lines stand for the sublattice magnetization $|m_A|$ (m_B), the solid lines for the total single-site magnetization $|m|$. Fig. 5b shows the temperature dependences of sublattice magnetization $|m_A|$ and m_B only, the insert shows the appropriate changes of total magnetization $|m|$.

Fig. 6 The time variation of dynamical autocorrelation function C_{auto}^{zz} when $E/J = 0.5$ is fixed and D/J changes: $D/J = -2.0$ (upper), 0.0 (central) and 1.0 (lower panel). The relevant time variations of C_{auto}^{zz} are displayed at three different temperatures, which are normalized with respect to their critical temperatures in order to get the ratio $\tau = 0.75, 1.0$ and 1.25 in Fig. 6ab and respectively, $\tau = 0.1, 0.25$ and 1.0 in Fig. 6c. Time axis is scaled in the \hbar/J unit.

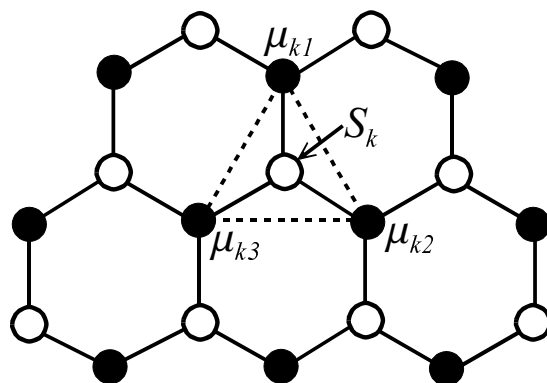


Fig. 1 Strecka et al.

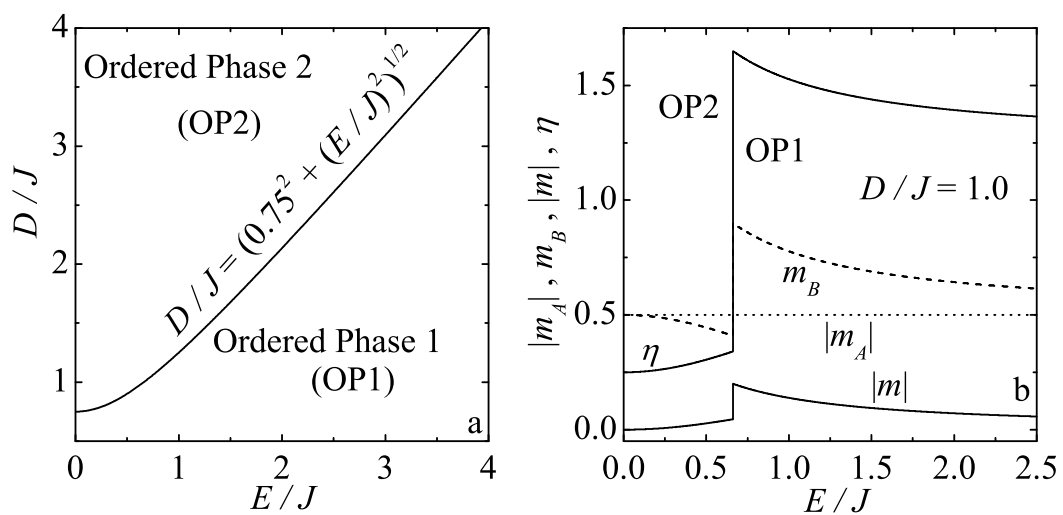


Fig. 2 Jascur et al.

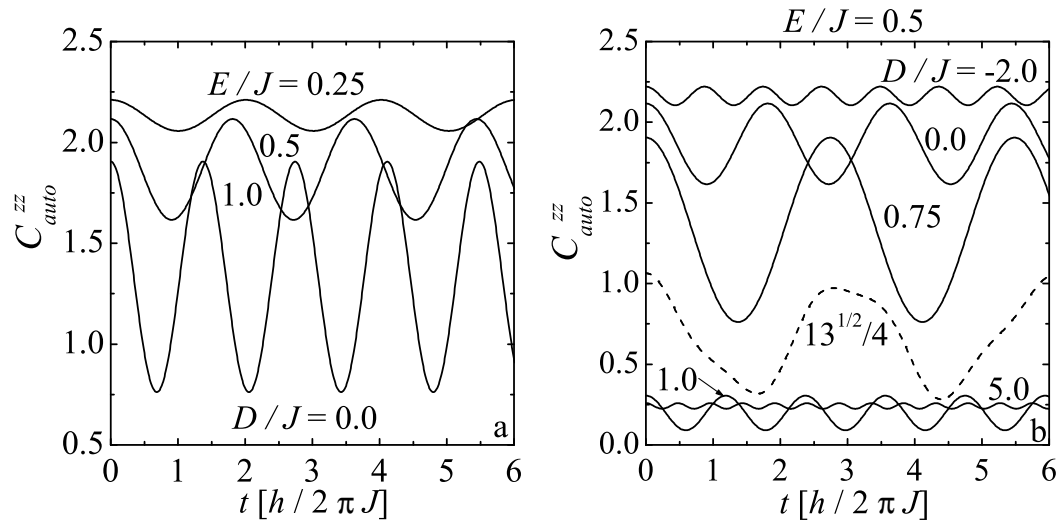


Fig. 3 Jascur et al.

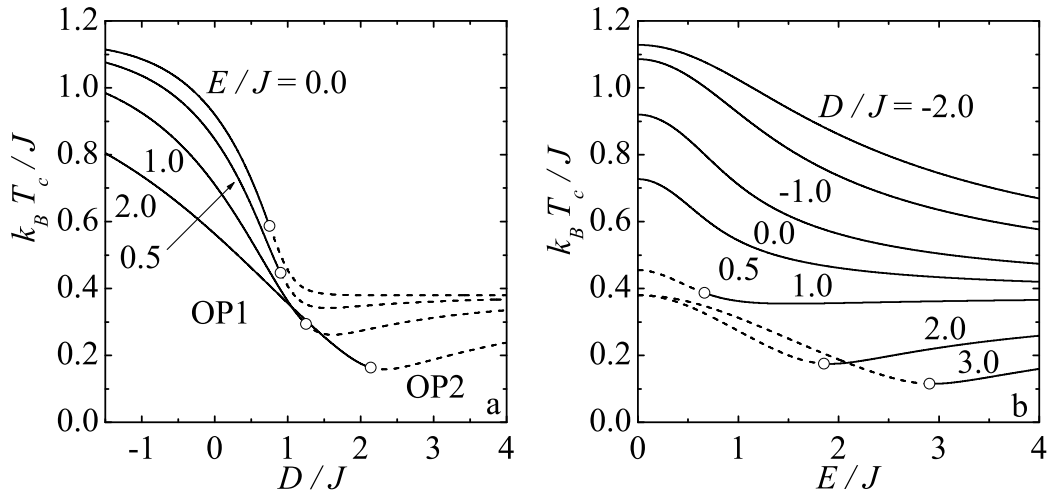


Fig. 4 Jascur et al.

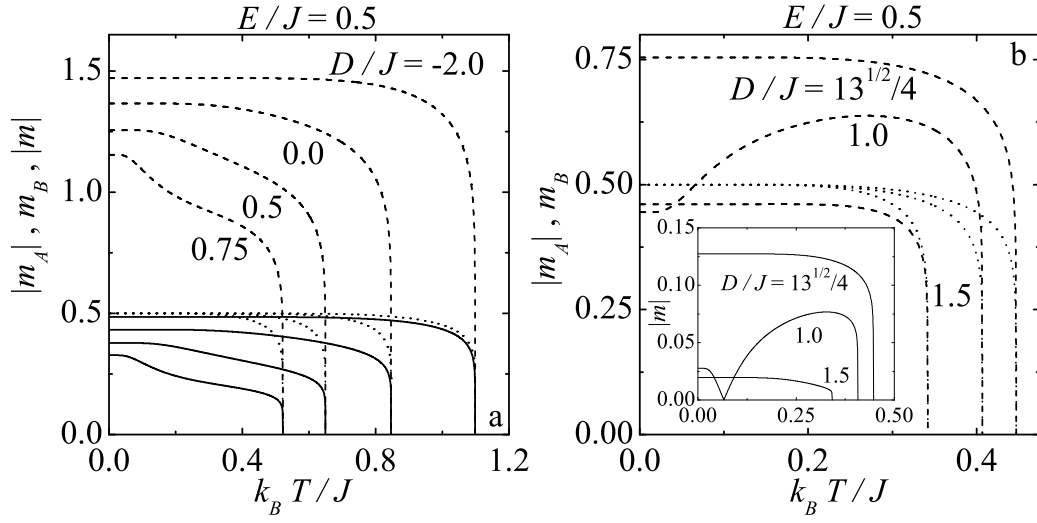


Fig. 5 Jascur et al.

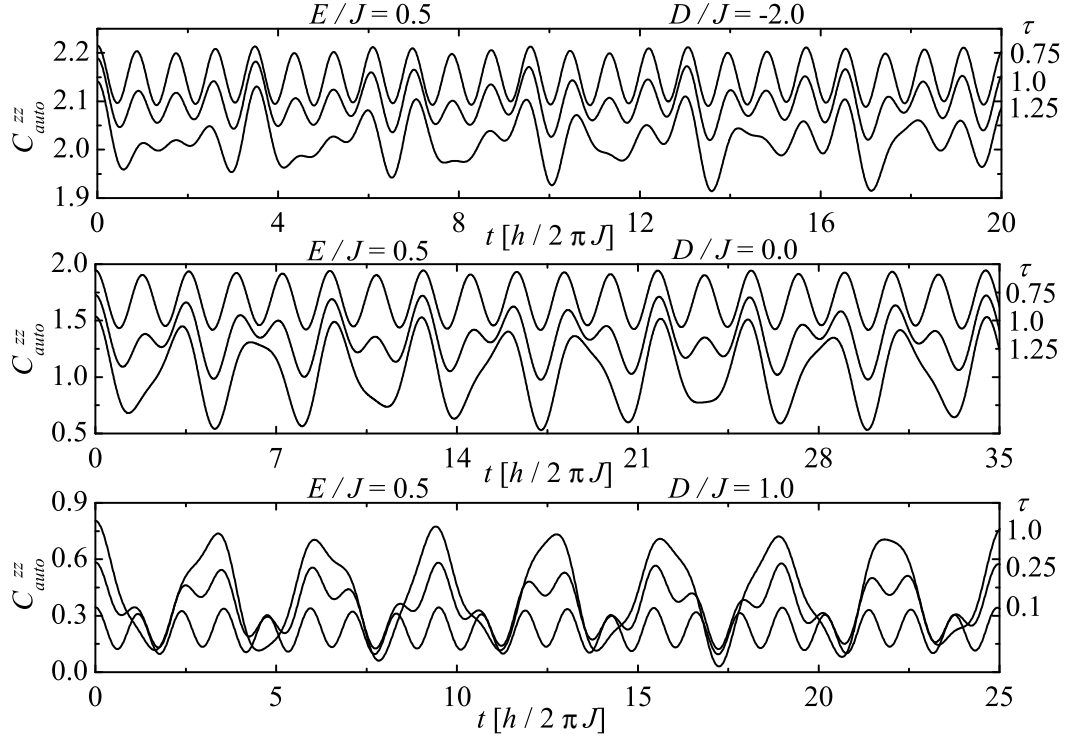


Fig. 6 Jascur et al.